Influence of the state of the Indian Ocean Dipole on following year's El Niño

Supplementary Information.

Takeshi Izumo[1,5], Jérôme Vialard[2], Matthieu Lengaigne[2], Clément de Boyer Montégut[3], Swadhin K. Behera[1], Jing-Jia Luo[1], Sophie Cravatte[4], Sébastien Masson[2] and Toshio Yamagata[1,5]

[1]Research Institute for Global Change, JAMSTEC, Yokohama, Japan

[2]LOCEAN, IRD-CNRS-UPMC, Paris, France

[3]LOS, IFREMER, Brest, France, formerly at JAMSTEC[1]

[4]LEGOS, IRD-CNRS-UPS, Toulouse, France

[5]University of Tokyo, Tokyo, Japan

Corresponding author address:

Dr. Takeshi Izumo

Ocean and Atmosphere group

Department of Earth and Planetary Sciences

Graduate School of Science, The University of Tokyo

Hongo 7-3-1, Bunkyo-ku, Tokyo 113-0033, Japan

E-mail: izumo@jamstec.go.jp

Supplementary information

In section 1 of the supplementary information, we provide a sketch and some explanations to summarize the mechanism that we propose to explain the influence of the state of the IOD on following year's El Niño, and introduce several additional arguments that support this mechanism. In section 2, we discuss our simple bilinear hindcast model in more detail (robustness, comparison with CGCM hindcasts, possible interdecadal variations). In section 3, we verify that the IOD phase tend to have a systematic relation with following year ENSO state using a composite analysis. In section 4, we provide more complete information on the various datasets and models used in this study. There are two tables and 6 figures in the supplementary information.

1. On the mechanism of ENSO triggering by preceding IOD

For simplicity, we will discuss the case of a negative IOD favouring an El Niño triggering, but the mechanism works also for a positive IOD that tends to favour La Niña conditions the following year (the analyses in this paper have also been done separately for negative and positive IOD cases, with similar results).

This section includes additional results (Figs S2 and S3) from the coupled general circulation model (CGCM) experiment and shallow water model described in section 4. The "noENSO" CGCM experiment has constrained SST over the tropical Pacific, in order to "kill" the Bjerknes feedback and ENSO variability, and allows identifying more clearly the remote signals associated with the IOD over the Pacific Ocean.

The mechanism of IOD influence on next year's ENSO state can be summarized in three main stages (Fig. S1):

a) In September-November of year 0, negative IOD conditions with warmer SST and increased convection in the eastern Indian Ocean and maritime continent (Fig. 2a, [Saji et al. 1999; Webster et al. 1999]) favour an enhanced Walker circulation of the Indo-Pacific region. These surface easterly anomalies over the Pacific in association with a negative IOD are suggested by observational analysis (Fig. 2c) and the CGCM "noENSO" experiment (Fig. 2d and top panels of Fig. S2). This agrees with a previous modelling study [Fischer et al. 2005] where another CGCM experiment with a constrained Pacific Ocean displays IOD-induced equatorial Pacific wind anomalies in October-November. Conceptually, Watanabe [2008]

demonstrated the essential role of the Indian Ocean in the Walker circulation state. This role is especially important during autumn when the observed maximum of tropical convection and precipitation, i.e. the center of the Walker circulation ascending branch, is over the eastern Indian Ocean; so the IOD eastern pole can significantly modulate the Walker circulation intensity during this season.

These surface wind easterly anomalies in the western-central equatorial Pacific force a downwelling Rossby wave and an upwelling Kelvin wave (Figs 3, S2 and S3). These waves increase the thermocline slope and induce a build-up of warm water in the western Pacific (Figs S2 and S3). In autumn, a positive warm water volume anomaly in the western Pacific is a precursor to following year's El Niño [Meinen and McPhaden 2000]. In addition, their reflection at both boundaries 2-3 months later will provide a positive feedback to El Niño development.

b) In December-February of year 0-1, the sudden demise of the IOD eastern pole and associated collapse of the Pacific easterly anomalies (Figs 2c-d and S2) forces a strong downwelling Kelvin wave (Figs 3, S2 and S3), which combines with the aforementioned reflected waves. The forced and reflected signals combine in the equatorial Pacific to produce positive sea level and zonal current anomalies (Figs 3, S2 and S3), overshooting the neutral equilibrium values [Cane 1979, McCreary and Anderson 1984]. This results in an eastward current anomaly which, in the western central Pacific, acts to displace the eastern edge of the warm pool eastward [e.g. Picaut et al. 1996], providing favourable grounds for El Niño to develop. A simple calculation of the SST anomalies resulting from advection by the currents of the shallow water experiment (Fig. 3) results in ~0.4°C anomalies over a 40° longitude fetch around the dateline between March and July, which seems sufficient to trigger the Bjerknes feedback [Palmer and Mansfield, 1984]. Wave reflections at both boundaries have previously been proposed to play a role in the ENSO cycle by providing a negative feedback to terminate El Niño in the delayed oscillator [Schopf and Suarez, 1988] and advective-reflective [Picaut et al., 1997] conceptual models. We propose here that the same mechanisms help the transition to an El Niño, in association with the IOD external forcing. The role of boundary reflection is probably slightly overestimated in our shallow water model, but previous studies have shown that wave reflections at both boundaries are highly efficient (90% and 75% reflection efficiency at the western and eastern boundaries, respectively [Boulanger and Menkes, 1999]).

c) From March-May of year 1, El Niño develops through the amplification of SST anomalies in the central Pacific by the Bjerknes feedback (the absence of the Bjerknes

feedback in "noENSO" explains the lack of ENSO development in this experiment, cf. Figs 2d and S2). This leads to a deeper thermocline and warmer SST along the oceanic equatorial wave-guide, coupled to increased convection at warm pool edge, anomalous westerlies to the west, and weakened Walker circulation to the east. The El Niño eventually peaks in following winter. In addition to the low-frequency mechanism discussed above, intraseasonal zonal wind variations may also promote the eastward migration of the warm pool, and favour El Niño development. The modified background state in the Western Pacific (eastward displacement of the warm pool and development of westerly wind and convection anomalies), and also in the south-equatorial Indian Ocean (the breeding ground for MJO onset), is associated with enhanced intraseasonal variability of the zonal winds [Zhang 2005; Eisenman et al. 2005; Vecchi et al. 2006; Izumo et al. 2010] that might also contribute to the ENSO development [e.g. Kessler et al. 1995, Lengaigne et al. 2004; McPhaden et al. 2006].

2. On the bilinear regression model

2.1 Testing other possible predictors

a) **The "best" predictor: an atmospheric convection-based IOD index.** The SST-based DMI index used in this study brings a good improvement of ENSO forecast at one-year lead. However, slightly better forecast can be obtained when using an IOD index based on Outgoing Longwave Radiation (OLR, a proxy of deep atmospheric convection) in October. This index was defined on the basis of partial regression of OLR in October with Niño3.4 at ENSO peak 14 months later, with the influence of October Pacific WWV removed. A very clear OLR dipole pattern, with increased convection in the eastern Indian Ocean, then appears and allows building an OLR-based IOD index [Izumo et al. 2010]. It is defined as the difference between OLR averaged over 80ºE-100ºE; 10ºS-5ºS and over 50ºE-70ºE; 5ºS-0º (using larger boxes, e.g. 80ºE-110ºE; 15ºS-5ºS and 30ºE-70ºE; 15ºS-15ºN, gives almost similar results, for example a hindcast correlation skill of 0.85 instead of 0.87 in second line of Table 1). This index is highly correlated with the DMI (0.91). This OLR index results in slightly better hindcast scores than the classical SST based DMI index (see Table 1), possibly for three reasons. One, the OLR index is more directly related to atmospheric convection and perturbations of the Walker circulation than the SST index is. Second, this OLR index is less subject to errors than the SST measurements that rely heavily on infrared estimates of the

SST, which are severely affected by cloud masking in heavy convective regions like the eastern Indian Ocean [Wentz 2000]. Third, the IOD is strongly phase-locked to the seasonal cycle, and taking the October value rather than the 3-months September-November averages might provide a better estimate of the IOD amplitude at its peak.

b) Poor efficiency of Pacific SST as a possible predictor. There is a strong association between ENSO and the IOD in boreal fall: a negative IOD is generally associated with a La Niña, and a positive IOD to an El Niño [e.g. Yamagata et al. 2004; Annamalai et al. 2005, and Fig. 1a]. One could thus wonder how an El Niño index would perform as an ENSO predictor compared to the DMI index we use. However, as underlined in many studies, El Niño indices have little predictive power beyond the spring barrier [e.g. Kessler 2002]. For instance, Niño3.4 SST in previous fall (SON) has a weak anti-correlation of -0.16 with ENSO peak 13 months later; and when combined with the WWV, it allows only a modest increase in skill score, compared to the improvement obtained when using IOD indices (see Table1). Figure 1 also shows that there is a significant correlation between the SON DMI and ENSO when DMI leads by 13-15 months, but that the opposite is not true. These analyses suggest that the DMI indeed influences the ENSO state at one year lead, but that the reverse is not true; and also that the DMI contains more information on the following year's ENSO state than the Pacific SST itself.

c) Sensitivity to other SST products. As seen in Table S1, the strong correlation between the DMI in SON and ENSO at 13 months lead is stable when using different SST products (ERSST or HadiSST) over the same 1981-2008 period, and so are the hindcast scores (not shown).

2.2 Performance in forecasting the different ENSO indices and ENSO types ("flavours")

As ENSO is a large scale coupled ocean-atmosphere phenomenon, various ENSO indices exist, based on oceanic (e.g. SST in various "Niño" regions) or atmospheric variables (e.g. the Southern Oscillation Index, SOI, the difference in sea level pressure between Darwin and Tahiti). Table S2 shows the skill of the bilinear regression model in hindcasting these various ENSO indices for Oct-Dec season. The bilinear model performs very well for most of these indices, with the best skill obtained for the SOI and for SST in the central Pacific (Niño4, Niño3.4 and Niño3). The skills are somewhat lower for extreme east (Niño1+2) and western Pacific SST indices (Niño5 and Niño6, with an expected opposite sign of the IOD influence), but are still significant at the 99% level.

Some recent studies highlighted that there may be different kinds of ENSO events, with some El Niños being weaker and with main SST anomalies in the central equatorial Pacific (called with various names such as El Niño "Modoki" type, e.g. the short review of Ashok and Yamagata 2009), and some others being stronger, with SST anomalies peaking in the central and eastern equatorial Pacific in boreal winter (e.g. "typical" El Niño).

Although the distinction between these various types (or "flavours") of El Niño remains highly debated, it may still be interesting to check the performance of the bilinear model in predicting these possible types of El Niño, as they appear to have different impacts on remote regions. The first lines of Table S2 show that our bilinear model has a good skill for SST in the different Niño regions, suggesting that it should have a good skill in forecasting the different El Niño "flavours". To go one step further, we tested the skill of the bilinear model to hindcast the El Niño Modoki index (EMI, Ashok et al. 2007), an index that can help to determine El Niño "flavour". It performs well with a 13 months-lead correlation skill of ~0.7. This suggests that the previous IOD may have a role in the occurrence of central Pacific El Niño Modoki type. Resolving this question would however require further investigations.

2.3 Performance of the bilinear regression compared to SINTEX-F CGCM forecasts. Extending the lead by combining them

This section first shows an example of comparison between the simple bilinear regression hindcasts and hindcasts based on the SINTEX-F CGCM [Luo et al. 2008]. Figure S4 compares the hindcasts of Niño3.4 SST in DJF of year 1 from 1st November of year 0 (14 months lead), from the bilinear regression model and from the SINTEX-F model. While both models perform well even before the so-called winter-spring predictability barrier, the simple bilinear regression model has a significantly better correlation skill (0.83) than the SINTEX-F model (0.61), even if the latter is one of the best forecasting system of ENSO at present [Jin et al. 2008]. However, the SINTEX-F hindcasts improve from the 1990s, possibly because of improvements in SST observations used in the assimilation scheme of the SINTEX-F model.

These two forecasting models can be exploited optimally by integrating the SINTEX-F forecasts of the IOD and of the WWV in fall within the bilinear regression model. This can allow to push even further ENSO predictability. For instance, using the SINTEX-F hindcasts from 1st August allow to have an excellent skill for the WWV in following fall, and a more moderate one for the IOD. Hence, using them results in a skill of 0.72/0.62/0.56, 15/16/17 months before ENSO peak when combining CGCM IOD and WWV hindcasts from the 1st of September/August/July with the bilinear model.

2.4 On possible past and future interdecadal changes

Several studies have suggested that there may have been changes in the teleconnections between the Pacific and Indian oceans before 1976 [e.g. Annamalai et al. 2005]. Such changes may however be partly unrealistic, because of changes in observational sampling density [e.g. Cox and Swail, 2001] and/or in measurement methods [e.g. Cardone et al. 1990] that could be misleading [e.g. Clarke and Lebedev 1996, Alory et al. 2005]. Concerning the present study, prior to 1980, subsurface observations in the tropical Pacific are too sparse to provide reliable estimates of the WWV, making it difficult to repeat the hindcast exercise for this period. We can however look at the stability of the one year lead IOD-ENSO relation in observations (subsection a) and in the SINTEX-F CGCM (subsection b) to investigate possible interdecadal changes in the IOD-ENSO relationship.

a) "Observed" interdecadal changes

Over the 1981-2008 period, all the IOD indices (DMI from 4 SST products, OLR IOD index and "Indian Oscillation Index" (IOI); see section 4.1) show a significant correlation (at the 99% level) with ENSO 14 months later (Table S1). This one year-lead correlation tends to be weaker over the 25 years period 1956-1980 than over the 1981-2008 period (Table S1). But when using the IOI or the DMI based on HadSST2 (HadSST2 is an uninterpolated SST product which only uses in situ data (not merged with satellites), and which may have reduced observational noise thanks to larger grid points (5ºx5º) compared to the other SST datasets), this correlation is relatively stable (the difference in correlation is not significant, even at the 70% level), remaining significant at the 95% level for the earlier period.

So this "observed" weakening could be due to the lower quality and sampling density of SST measurements. The former issue is crucial because of the lack of past SST observations, especially for the narrow autumn seasonal window of the small DMI eastern pole (only about 2 to 4 observations per month per 2º by 2º box in most of that region before the end of the 1990s; from International Comprehensive Ocean-Atmosphere Data Set (ICOADS), not shown). This observational issue is well illustrated by comparing the interannual variability of the DMI eastern pole SST in Sept-Nov to the better-observed variability of the OLR eastern pole, available over the 1974-2008 period. Their correlation is excellent, 0.92, for the well-observed second half of the period (1991-2008), but is much lower, 0.39, for the first half (1974-1990). This suggests that SST observational data were strongly lacking before the 1990s to accurately estimate the DMI, likely contributing to the apparent "observed" interdecadal change.

Part of the "observed" weakening could also be real. Natural interdecadal fluctuations independent of anthropogenic climate change could already explain part of such interdecadal changes, as suggested by the following model analysis. Furthermore, coral records show long-term variations and an increasing trend in IOD occurence [Abram et al. 2008]. This possible trend, maybe attributable to climate change, might favour a stronger IOD influence on following year's ENSO. Further studies are needed to resolve such issue.

b) Interdecadal variations in the SINTEX-F CGCM

The CGCM control experiment provides a long record over which to test the hindcast model that we have built to predict the ENSO peak in observations. We have built a series of similar hindcast models on 30-years long sliding window in this CGCM experiment. Figure S5 shows the resulting hindcast scores. The bilinear regression correlation skill and the IOD and WWV contributions have notable interdecadal variations over 30-years long periods. Over some periods (e.g. years 90-110), the CGCM has a behaviour consistent with the 1981-2008 period in observations (i.e. a strong skill score of ~ 0.8, with a strong contribution from the Indian Ocean), while both the skill score and importance of the Indian Ocean weaken during some other periods (e.g. years 180 to 200). While this model analysis has also its limits (the CGCM might suffer from climate drift, or its interdecadal variations might not be realistic), it suggests that the influence of the IOD on following year's ENSO state, while being strong and highly significant in average, might fluctuate interdecadally.

3. Composite analysis

In the present paper, we mostly used linear regressions to show the signals related to an IOD event. We use in this section the composite method, which is often used in climate science, so as to verify that the results shown in the present paper are independent of the statistical method used.

3.1 Definitions of IOD and ENSO years

We first need to define IOD and ENSO years. We used the standard IOD and ENSO indices presented in the methods section, i.e. the DMI in Sept-Nov and the Niño3.4 SST in Oct-Dec. We then selected anomalous years when the index anomaly had an absolute value greater than two thirds of its standard deviation. Over the Sep. 1981- Dec. 2008 period, there

were 6 negative IOD (1981, 1990, 1992, 1996, 1998, 2005), 5 positive IOD (1982, 1991, 1994, 1997, 2006), 8 El Niño (or possibly El Niño "Modoki" such as 1994) events (1982, 1986, 1987, 1991, 1994, 1997, 2002, 2006) and 8 La Niña events (1983, 1984, 1988, 1995, 1998, 1999, 2000, 2007).

3.2 Composites

To test the lead-relationship of IOD state with following year's ENSO, the composites can be done in two ways. One way is to do composites of the oceanic and atmospheric conditions one year after a negative or positive IOD event (upper panels of Fig. S6). The other way is to do composites of the conditions one year before an El Niño or a La Niña event (lower panels of Fig. S6). The upper panels display typical El Niño (La Niña) conditions one year after negative (positive) IOD events. The lower panels show typical negative (positive) IOD anomalies one year before El Niño (La Niña) conditions. This composite analysis confirms that a negative (positive) IOD state in fall will favour the occurrence of El Niño (La Niña) conditions the following year.

4. Detailed description of data and models

4.1 Observational datasets

We used NOAA OI SST v2 data [Reynolds et al. 2002] for Nov.1981-Aug.2009, and HadiSST v1.1 [Rayner et al. 2003] prior to Nov.1981, to assess SST interannual variability. We also used HadSST2 (uninterpolated product, [Rayner et al. 2006]) and ERSST v3b (interpolated, [Smith and Reynolds 2004]), both based only on in situ observations (no merging with satellital measurements), for comparison. To estimate SST changes for the shallow water model, we used TMI SST for 1998-2007 [Wentz et al. 2000] to obtain an accurate estimate of the climatological SST gradient in the equatorial Pacific.

Outgoing Longwave Radiation (OLR) is a classical proxy for deep convection in the tropics and widely used to characterize the MJO. We use the daily 2.5°×2.5° interpolated product from NOAA [Liebmann and Smith 1996] available from 1974 to 2008 (with a gap in 1978).

For wind variability, the 10 m winds and surface windstress from NCEP2 reanalysis [Kanamitsu et al. 2002] are used (available from 1979). When analysing windstress high-frequency (for Fig. 4), a 3 points spatial Hanning filter, removing wavelengths lower than 1.5º, was applied so as to reduce the observational noise.

Tropical Pacific Warm Water Volume index (WWV, [Meinen and McPhaden 2000], based on thermal analyses produced by BMRC, including TAO/TRITON array observations [McPhaden et al. 1995]) is used to assess recharge-discharge processes for the entire equatorial band (available at http://www.pmel.noaa.gov/tao/elNiño/wwv/ from august 1980). Temperature averaged over the first 300 m ("T300", proportional to ocean heat content) and related thermocline depth variations along the equatorial Indo-Pacific are investigated using firstly an oceanic reanalysis produced by the CERFACS [Weaver et al. 2005; Daget et al. 2008] within the ENSEMBLES project. Note that sensitivity tests using sea level anomaly from TOPEX/Poseidon and JASON satellites (AVISO product) or the SODA-POP ocean reanalysis [Carton and Giese 2008] give similar results (e.g. for Fig. 2b and for the bilinear hindcast model).

We also used the "Indian Oscillation Index" (IOI), defined as the difference of sea level pressure between Seychelles (4.40ºS, 55.27ºE) and Darwin, less subject to observational uncertainties [Marsac and LeBlanc 1998]. Note however that there were some changes in IOI western pole location before 1972, the difference Seychelles-Darwin being padded with the difference Agalega (an Island south of the Seychelles archipelagos at 10ºS) minus Darwin when Seychelles data were missing.

4.2 SINTEX-F CGCM and noENSO experiment

The coupled model used is the SINTEX-F (Scale Interaction Experiment-FRCGC) global ocean-atmosphere CGCM [Masson et al. 2005, Luo et al. 2003; 2005], developed at Frontier Research Center for Global Change (FRCGC, renamed RIGC) under the European Union-Japan collaboration. The oceanic component is the OPA (Ocean Parallelise, renamed NEMO) Ocean GCM (OGCM) in its 8.2 version [Madec et al. 1998], with a resolution of 2º in longitude, from 0.5º (near the equator) to 2º in latitude (ORCA2 grid) and of 10 m vertically in the first 150 m. The atmospheric component is the ECHAM 4.6 [Roeckner et al. 1996] Atmosphere GCM (AGCM) with a high horizontal resolution of 1.125º x 1.125º (T106 spectral grid) and 19 hybrid sigma-pressure levels in the vertical. Computations were performed on the Japanese Earth Simulator, with improved coupling physics [Luo et al. 2005]

and without flux corrections. At least 70 years were computed for each experiment, so that seasonal cycles and regressions could be calculated over 50 years (years 21 to 70), after the removal of the first 20 years of spin up. The CTL experiment was run for more than 200 years (e.g. Fig. S5). This CGCM simulates quite realistically the ENSO and IOD phenomena, and is extensively used to study and forecast them [Luo et al. 2005, 2007, 2008; Behera et al. 2006]. However, because of spatial [Luo et al. 2005] and seasonal [Tozuka et al. 2005] biases in the simulated ENSO variability, ENSO peak is better defined as Niño3 SST in DJF in this CGCM (definition used in Fig. S5). For details and for further validations of the CGCM version used here, readers are referred to previous publications [Masson et al. 2005; Luo et al. 2005, 2007].

In a sensitivity experiment ("noENSO"), the atmospheric component of the CGCM only feels the 50-year mean seasonal SST of the control experiment (CTL) over the tropical Pacific (from 120ºE-130ºE to Pacific eastern boundary) instead of the interannually varying SST of the oceanic component, hence removing the ocean-atmosphere coupling in the tropical Pacific, and consequently ENSO variability (see Behera et al. 2006 for an extended description of this experiment).

4.3 Shallow water model

The shallow water model consists of a upper layer with mean depth H and density ρ overlying a deep lower layer of density $\rho + \Delta\rho$. Linear equations of motion are similar to those described in McCreary and Anderson [1984]. In the present study, H is 100 m, roughly consistent with the mean thermocline depth in the equatorial Pacific Ocean. The reduced gravity is 0.062 m s^{-2}, in order to have a realistic Kelvin wave speed c=2.5m s^{-1} similar to the observed celerity of the first baroclinic mode [e.g. Delcroix et al. 1991]. The horizontal mixing coefficient is chosen here as 500 m^2 s^{-1} [e.g. Lengaigne et al. 2003]. The idealized basin representing the tropical Pacific has a western boundary at 130°E (the average latitude of wave reflection [Boulanger and Menkes 1999]) and an eastern boundary at 80°W.

The shallow water model allows assessing the thermocline depth and ocean current responses to wind forcing. We added a simple thermal equation to estimate SST anomalies. These are dominated by zonal advection effects in the central Pacific [e.g. Picaut et al. 1996; Vialard et al. 2001], vertical advection effects becoming important towards the eastern Pacific (where the effects of thermocline vertical movements dominate). The latter effects are estimated by using a simplified form proportional to the thermocline depth anomaly H'. The simplified mixed layer temperature tendency equation has the form:

$\partial T'/\partial t = -U' \ \partial \langle T \rangle / \partial x + \alpha \ (\gamma \ H' - T')$

T is the SST, U the surface zonal current, H the thermocline depth, T', U' and H' their anomalies, brackets denote climatological values. α represents a damping term (mostly through the negative feedback of surface fluxes), and γ the efficiency of vertical advection. α and γ can be estimated from observations (here estimated from Burgers et al. 2005). For simplification, α is chosen constant, $\alpha = (2.75 \ \text{months})^{-1}$ (choosing other values of the same order does not change the main results). And γ is scaled by the strength of the upwelling, estimated from climatological zonal wind stress $\langle \tau_x \rangle$, the effect being stronger when the upwelling is stronger [McPhaden 2002]: $\gamma = \gamma_0 \ \langle \tau_x \rangle / (\langle \tau_x \rangle_{170°W-95°W})$, where $\gamma_0 = 0.0077$ K/m and $\langle \tau_x \rangle_{170°W-95°W}$ is the climatological equatorial wind stress averaged over 170ºW-95ºW. The resulting SST change is only weakly influenced by the vertical term in the western-central Pacific. Using an even more simplified equation without the vertical advection term therefore leads to similar results in the western-central Pacific (not shown). Whereas the above equation does not pretend to evaluate accurately SST anomalies in the eastern Pacific it is appropriate for the central Pacific, which is the key region for the development of the Bjerknes feedback.

In this paper, we presented the result of one experiment. An idealized patch of anomalous easterly wind stress is applied to mimic the observed intensification of the easterlies associated with the IOD. This wind patch (a Gaussian centred at 0°N, 180°E, with e-folding widths of 40º in longitude and 7.5º in latitude, and with a maximal amplitude of -0.01 N m^{-2}) is applied from September to November.

References for Supplementary Information

Abram, N.J., M. K. Gagan, J. E. Cole, W. S. Hantoro & M. Mudelsee, 2008: Recent intensification of tropical climate variability in the Indian Ocean, *Nature Geoscience*, **1**, 849-853.

Alory, G., S. Cravatte, T. Izumo and K. Rodgers, 2005:Validation of a decadal OGCM simulation for the tropical Pacific. *Ocean Modelling*, **10**, 272-282.

Annamalai, H., S.-P. Xie, J.-P. McCreary & R. Murtugudde, 2005: Impact of Indian Ocean sea surface temperature on developing El Niño. *J. Clim*. **18**, 302–319.

Ashok, K., S. K. Behera, S. A. Rao, H. Weng, and T. Yamagata, 2007: El Niño Modoki and its possible teleconnection. J. Geophys. Res., 112, C11007, doi:10.1029/2006JC003798.

Ashok, K., and T. Yamagata, 2009 : The El Niño with a difference. *Nature*. **461**, 481-484.

Behera, S. K., J.J. Luo, S. Masson, S. A. Rao, H. Sakuma & T. Yamagata, 2006: A CGCM study on the interaction between IOD and ENSO, *J. Clim.*, **19**, 1608-1705.

Boulanger, J.-P., & C. Menkes, 1999: Long equatorial wave reflection in the Pacific Ocean during the 1992-1998 TOPEX/POSEIDON period, *Clim. Dyn.* **15**, 205-225.

Burgers, G., F.-F. Jin, and G. J. van Oldenborgh, 2005: The simplest ENSO recharge oscillator, *Geophys. Res. Lett.*, **32**, L13706, doi:10.1029/2005GL022951.

Cane M.A., 1979: Response of an equatorial ocean to simple wind stress patterns .2. Numerical results. *J. Marine Res*. **37** (2), 253-299.

Cardone, V.J., Greenwood, J.G., Cane, M.A., 1990. On trends in historical marine wind data. *J. Climate* **3**, 113–127.

Carton, J.A., and B.S. Giese, 2008: A reanalysis of ocean climate using Simple Ocean Data Assimilation (SODA), *Mon. Wea. Rev.*, **136**,2999-3017.

Clarke, A.J., Lebedev, A., 1996. Long term changes in the equatorial Pacific trade winds. *J. Climate* **9**, 1020–1029.

Cox, A.T., Swail, V.R., 2001. A global wave hindcast over the period 1958–1997: validation and climate assessment. *J. Geophys. Res.* **106**, 2313–2329.

Daget, N., Weaver, A. T. and M. A. Balmaseda, 2008: An ensemble three-dimensional variational data assimilation system for the global ocean: sensitivity to the observation- and background-error formulation. *ECMWF Tech. Memo.* **562**.

Delcroix, T., J. Picaut, and G. Eldin, 1991: Equatorial Kelvin and Rossby waves evidenced in the Pacific Ocean through geosat sea level and surface current anomalies, *J. Geophys. Res.*, **96**, 3249–3262.

Eisenman, I., L. Yu and E. Tziperman, 2005: Westerly Wind Bursts: ENSO's Tail Rather than the Dog? *J. Clim.*, **18,** 5224-5238.

Fischer, A., P. Terray, E. Guilyardi, S. Gualdi, and P. Delecluse, 2005: Two independent triggers for the Indian Ocean Dipole/Zonal Mode in a coupled GCM, *J. Clim*., **18**, 3428 – 3449.

Izumo, Masson S., Vialard J., C. de Boyer Montegut, S. K. Behera, G. Madec, K. Takahashi & T. Yamagata, 2010: Low and high frequency Madden-Julian Oscillations in Austral Summer - Interannual variations. *Clim. Dyn.*, in press, published online.

Jin E. K., James L. Kinter III, B. Wang, C.-K. Park, I.-S. Kang, B. P. Kirtman, J.-S. Kug, A. Kumar, J.-J. Luo, J. Schemm, J. Shukla, T. Yamagata, 2008: Current status of ENSO prediction skill in coupled ocean–atmosphere models. *Clim Dyn.*, **31**, 647–664.

Kanamitsu, M., Ebisuzaki, W., Woollen, J., Yang, S.-K., Hnilo, J. J., Fiorino, M., and Potter, G. L., 2002: NCEP-DOE AMIP-II reanalysis. *Bull. Amer. Meteor. Soc*., **83**, 1631-1643.

Kessler, W. S., M. J. McPhaden, and K. M. Weikmann, 1995: Forcing of intraseasonal Kelvin waves in the equatorial Pacific, *J. Geophys. Res*., **100**, 10,613–10,631.

Kessler, W. S., 2002: Is ENSO a cycle or a series of events?, *Geophys. Res. Lett*., **29**(23), 2125, doi:10.1029/2002GL015924.

Lengaigne M., G. Madec, C. Menkes and G. Alory, 2003: Impact of isopycnal mixing on the tropical ocean circulation, *J. Geophys. Res*., **108**, 3345–3358.

Lengaigne, M., J.-P. Boulanger, C. Menkes, P. Delecluse, & J. Slingo, 2004: Westerly wind events in the tropical Pacific and their influence on the coupled ocean-atmosphere system: A review, in Earth Climate: The Ocean-Atmosphere Interaction, *Geophys. Monogr. Ser.,* **147**, 49– 69, AGU, Washington, D. C.

Liebmann, B., and C. A. Smith, 1996: Description of a complete (interpolated) outgoing longwave radiation dataset. *Bull. Amer. Meteor. Soc*., **77**, 1275–1277.

Luo, J.-J., S. Masson, S. Behera, P. Delecluse, S. Gualdi, A. Navarra, and T. Yamagata, 2003: South Pacific origin of the decadal ENSO-like variation as simulated by a coupled GCM. *Geophys. Res. Lett.,* **30,** 2250, doi:10.1029/2003GL018649

Luo, J.-J., S. Masson, E. Roeckner, G. Madec and T. Yamagata, 2005: Reducing climatology bias in an ocean-atmosphere CGCM with improved coupling physics. *J. Climate*, **18¸** 2344-2360.

Luo, J.-J., S. Masson, S. Behera, and T. Yamagata, 2007: Experimental Forecasts of the Indian Ocean Dipole Using a Coupled OAGCM, *J. Climate*, **20**, 2178–2190.

Luo, J.-J., S. Masson, S.K Behera and T. Yamagata, 2008 : Extended ENSO predictions using a fully coupled ocean atmosphere model. *J. Climate*, **21**, 84-93.

Madec, G., P. Delecluse, M. Imbard and C. Levy, 1998: OPA 8.1 Ocean General Circulation Model reference manual. Notes du pôle de modélisation de l'IPSL 11, 91pp., available at http://www.lodyc.jussieu.fr/opa.

Masson, S. et al., 2005: Impact of barrier layer on winter-spring variability of the southeastern Arabian Sea, *Geophys. Res. Lett.*, **32**, L07703, doi:10.1029/2004GL021980.

Marsac, F. and J-L. Le Blanc, 1998: Interannual and ENSO-associated variability of the coupled ocean-atmosphere system with possible impacts on the yellowfin tuna fisheries of the Indian and Atlantic Oceans. Tuna Symposium, Pta Delgada, Acores, 10-18 Juin 1996. Coll. Vol. Scient. Papers, Vol L(2):345-377

McCreary, J.P., and D.L.T. Anderson, 1984: A simple model of El Niño and the Southern Oscillation. *Mon. Wea. Rev.*, **112**, 934-946.

McPhaden, M. J., 1995: The tropical atmosphere ocean array is completed. *Bull. Am. Meteorol. Soc.*, **76**, 739–741.

McPhaden, M. J., 2002: Mixed layer temperature balance on intraseasonal timescales in the equatorial Pacific Ocean, *J. Clim.*, **15**, 2632 – 2647.

McPhaden, M.J., X. Zhang, H.H. Hendon, & M.C. Wheeler, 2006: Large Scale Dynamics and MJO Forcing of ENSO Variability. *Geophys. Res. Lett.*, **33**(16), L16702, doi:10.1029/2006GL026786.

Meinen, C.S. and M.J. McPhaden, 2000: Observations of warm water volume changes in the equatorial Pacific and their relationship to El Niño and La Niña. *J. Clim.*, **1**3, 3551-3559.

Palmer T.N. and Mansfield D.A., 1984: Response of two atmospheric general circulation models to sea-surface temperature anomalies in the tropical East and West Pacific. *Nature* **310**(5977): 483.

Picaut J., Ioualalen M., Menkes C., Delcroix T. and M.J. McPhaden, 1996: Mechanism of the zonal displacements of the Pacific warm pool: implications for ENSO, *Science*, **274**, 1486-1489.

Picaut, J., F. Masia, and Y. du Penhoat, 1997: An advective-reflective conceptual model for the oscillatory nature of the ENSO, *Science*, **277**, 663–666.

Rayner, N. A.; Parker, D. E.; Horton, E. B.; Folland, C. K.; Alexander, L. V.; Rowell, D. P.; Kent, E. C.; Kaplan, A., 2003: Global analyses of sea surface temperature, sea ice, and night marine air temperature since the late nineteenth century, *J. Geophys. Res.*, **108**, No. D14, 4407 10.1029/2002JD002670

Rayner, N.A., P.Brohan, D.E.Parker, C.K.Folland, J.J.Kennedy, M.Vanicek, T.Ansell and S.F.B.Tett, 2006: Improved analyses of changes and uncertainties in sea surface temperature measured *in situ* since the mid-nineteenth century: the HadSST2 data set. *J. Clim.* **19**(3) pp. 446-469.

Reynolds, R. W., N. A. Rayner, T.M. Smith, D. C. Stokes and W. Wang, 2002: An improved in situ and satellite SST analysis for climate. *J. Clim.*, **15**, 1609-1625.

Roeckner, E. and Coauthors., 1996: The atmospheric general circulation model ECHAM-4: Model description and simulation of present-day climate. *Max-Planck-Institut für Meteorologie Rep.*, **218**, 90 pp.

Saji, N. H., B. N. Goswami, P. N. Vinayachandran & T. Yamagata, 1999: A dipole mode in the tropical Indian Ocean. *Nature* **401**, 360-363.

Schopf P.S. and M.J. Suarez, 1988: Vacillations in a coupled ocean-atmosphere model. *J Atmos Sci.*, **45**, 549-566.

Smith, T. M., and R. W. Reynolds, 2004: Improved extended reconstruction of SST (1854-1997). *J. Clim.*, **17**, 2466-2477.

Vecchi, G.A., A.T. Wittenberg and A. Rosati, 2006: Reasessing the role of stochastic forcing in the 1997-8 El Niño. *Geophys. Res. Lett.,* **33**, L01706, doi:10.1029/2005GL024738.

Vialard, J., C. Menkes, J.-P. Boulanger, P. Delecluse, E. Guilyardi, M.J. McPhaden and G. Madec, 2001: A model study of oceanic mechanisms affecting equatorial Pacific sea surface temperature during the 1997–98 El Niño, *J. Phys. Oceanogr.*, **31**,1649–1675.

Watanabe, M., 2008: Two regimes of the equatorial warm pool. Part I: A simple tropical climate model. *J. Climate*, **21**, 3533–3544.

Weaver, A. T., Deltel, C., Machu, E., Ricci, S. and N. Daget, 2005: A multivariate balance operator for variational ocean data assimilation. *Q. J. Roy. Meteo. Soc.*, **131**, 3605-3625.

Webster, P. J., A. M. Moore, J. P. Loschnigg, & R. R. Leben, 1999: Coupled oceanic–atmospheric dynamics in the Indian Ocean during 1997–98. *Nature*, **401**, 356–360.

Wentz F. J., Gentemann C., Smith D., & Chelton D., 2000: Satellite Measurements of Sea Surface Temperature Through Clouds, *Science* **288**, 847.

Yamagata, T., S. K. Behera, J.J. Luo, S. Masson, M. R. Jury, & S. A. Rao, 2004: Coupled Ocean-Atmosphere variability in the Tropical Indian Ocean, Earth's climate: The Ocean-Atmosphere Interaction. *Geophys. Monogr. Ser.* **147** AGU, Washington, D. C.

Zhang, C., 2005: Madden-Julian Oscillation, *Rev. Geophys.*, **43**, RG2003, doi:10.1029/2004RG000158.

Supplementary Figures
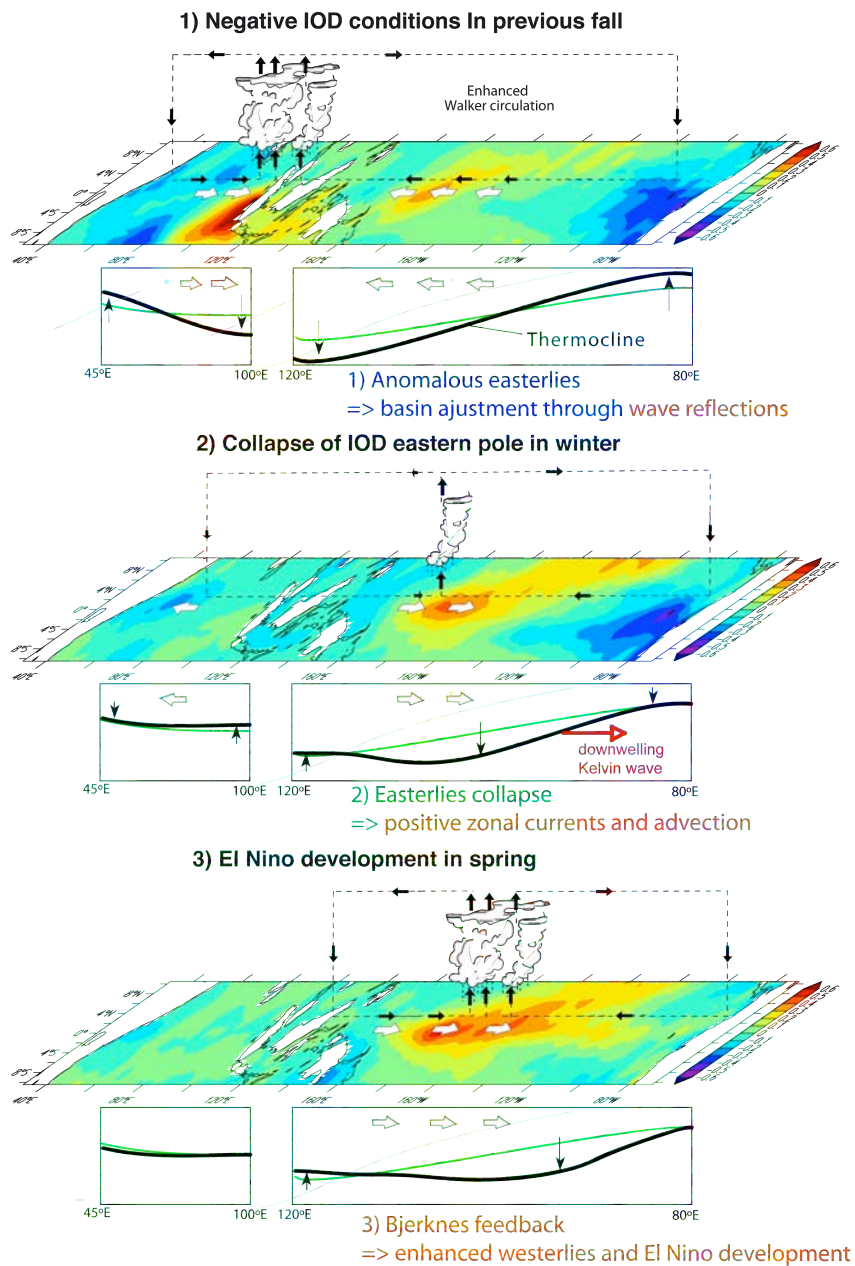
Fig. S1: Schematic summarizing the main mechanism of how previous year IOD conditions can influence ENSO triggering. The anomalous SST related to negative IOD conditions in fall of year 0 (regression similar to Fig. 2a) is shown in color (ºC) for the tropical Indo-Pacific region. The anomalous surface winds are represented schematically by black arrows. The Walker cell is represented schematically by a dashed line. Changes in thermocline depth along the equator are schematized as a thick black line (compared to normal conditions in thin green line), while black arrows represent thermocline vertical displacements, and white arrows the near-surface currents.

17
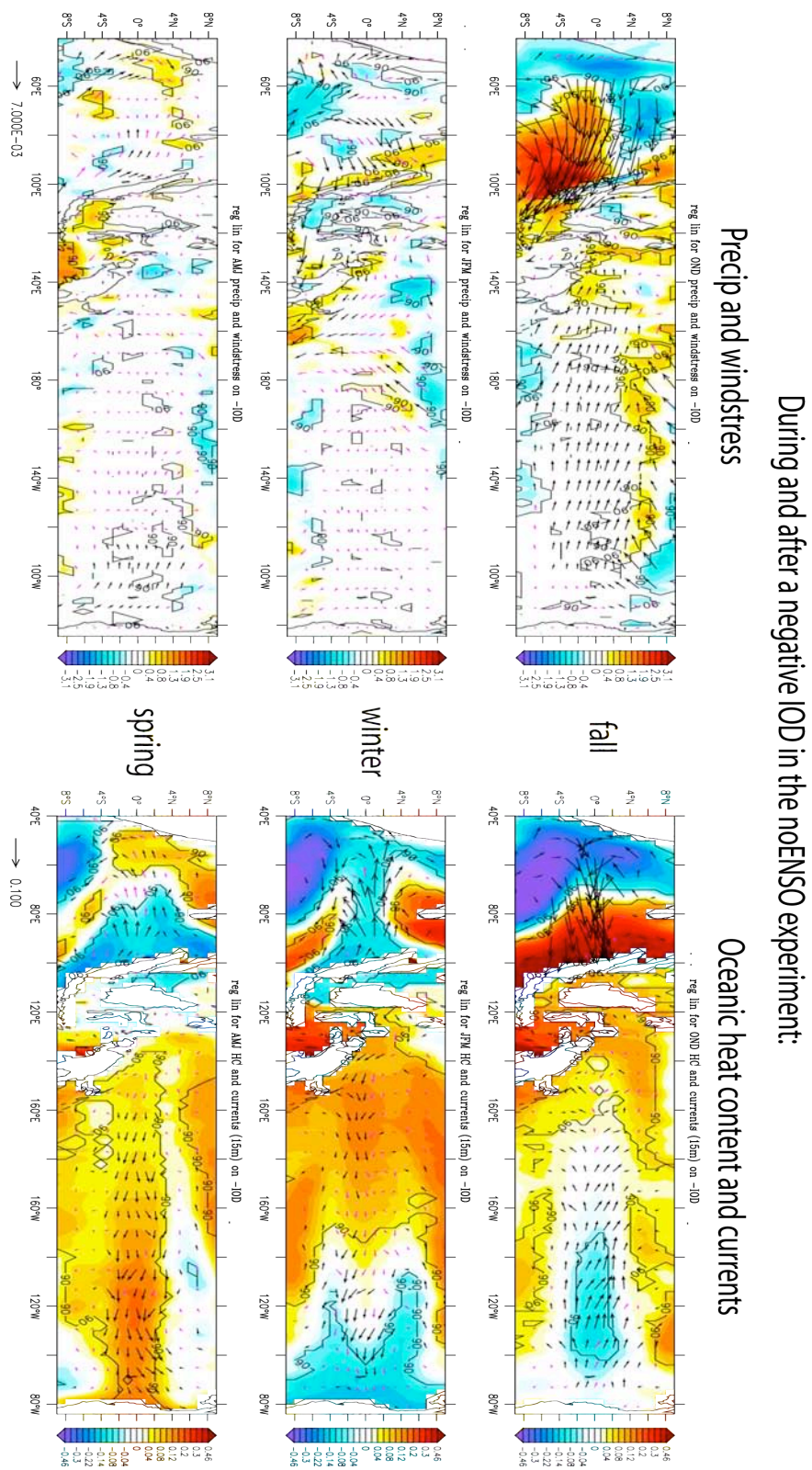
Fig. S2: SST and windstress (left), and ocean heat content and currents (right) regressed on – IOD (-DMI in SON) in fall, spring and winter, in the noENSO experiment. The 90% significance level is indicated in black contours for SST and ocean heat content, and by black vectors for wind stress and currents. Note the logarithmic-like scale used for shading because of the large range of significant values.
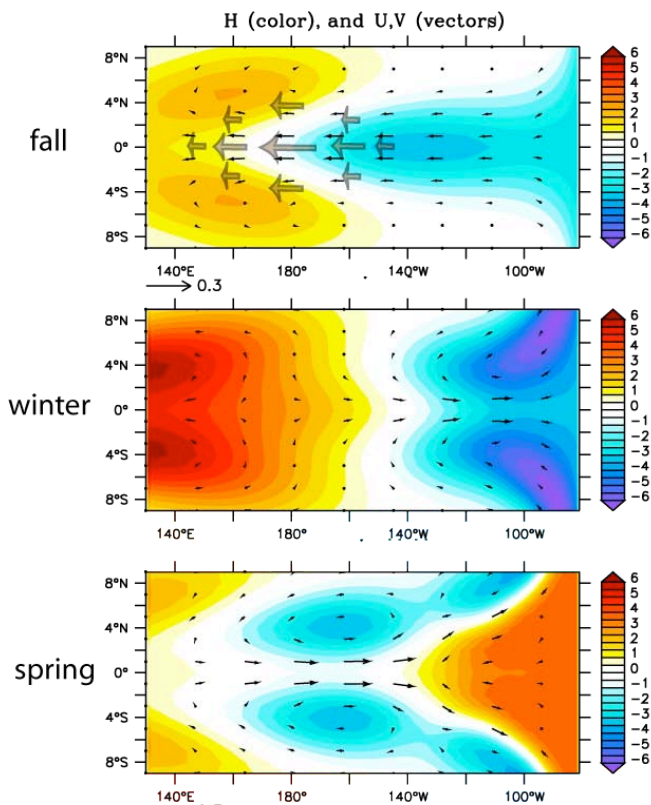
Fig. S3: Maps of the thermocline depth and surface current anomalies in the shallow water model in the Pacific Ocean for fall (upper, SON), winter (middle, DJF) and spring (lower, MAM), for the experiment forced by easterly anomalies (schematized by half-transparent brown arrows) associated with the negative IOD in fall.

observed Nino3.4 SST in DJF one year later (black), its bilin. reg. hindcasts (red, correl. 0.83) and SINTEX−F hindcasts (green, correl. 0.61) from 1st nov.
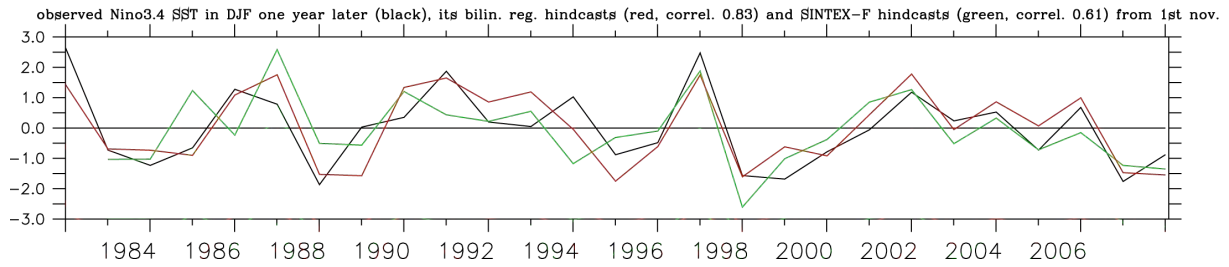
Fig. S4: Similar to Fig. 1c, but here comparing the hindcasts of Niño3.4 SST in Dec.-Feb. from 1st November (15 months lead) of the bilinear regression model (red, using October OLR-IOD index and WWV) and of the SINTEX-F model (green, Luo et al. 2008). Here the hindcasts have been renormalized, so as to have the same standard deviation as observations (black) and to allow their comparison.

Interdecadal fluctuations of the ENSO peak hindcast score, and of DMI and WWV contributions, in SINTEX-F CGCM
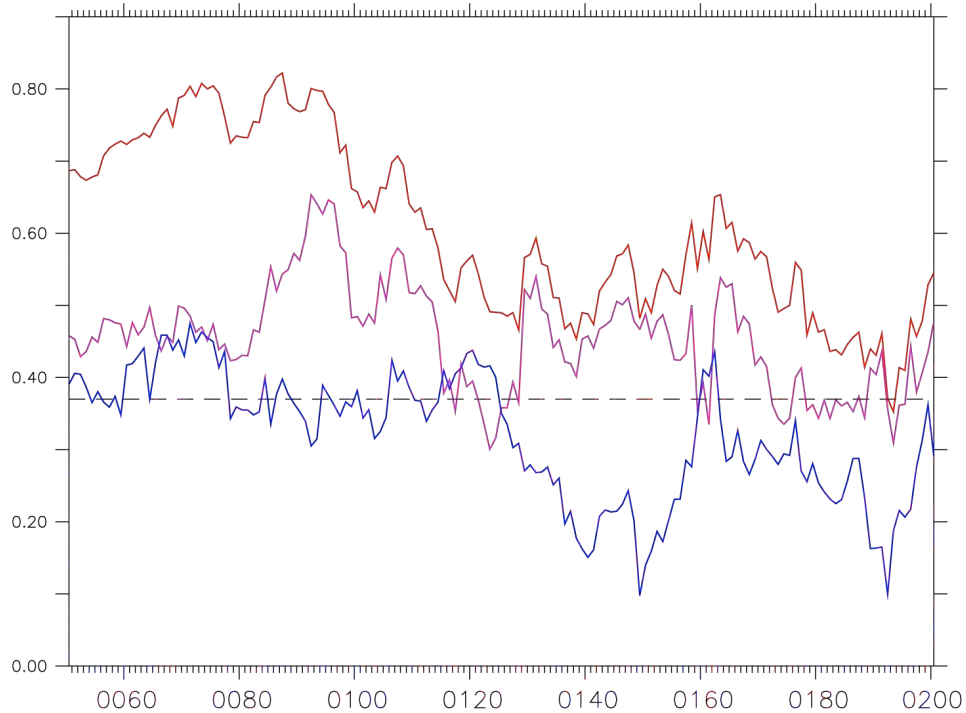
Figure S5: Interdecadal fluctuations of the IOD influence on following year's ENSO state over 150 years in the control experiment of the SINTEX-F CGCM. Hindcast skill score of ENSO peak using DMI+WWV in Sept-Nov with a 15 months lead over 30 years sliding windows (red). 15 months lead correlations of DMI (purple) and WWV (blue) with ENSO peak, over 30 years-long sliding windows. For the entire corresponding period, the hindcast correlation score is 0.59, with lead-correlations of DMI and WWV respectively of -0.46 and 0.31 (significant at the 99.9% level). The dashed line indicates the 95% confidence level for correlations over 30 years-long periods.
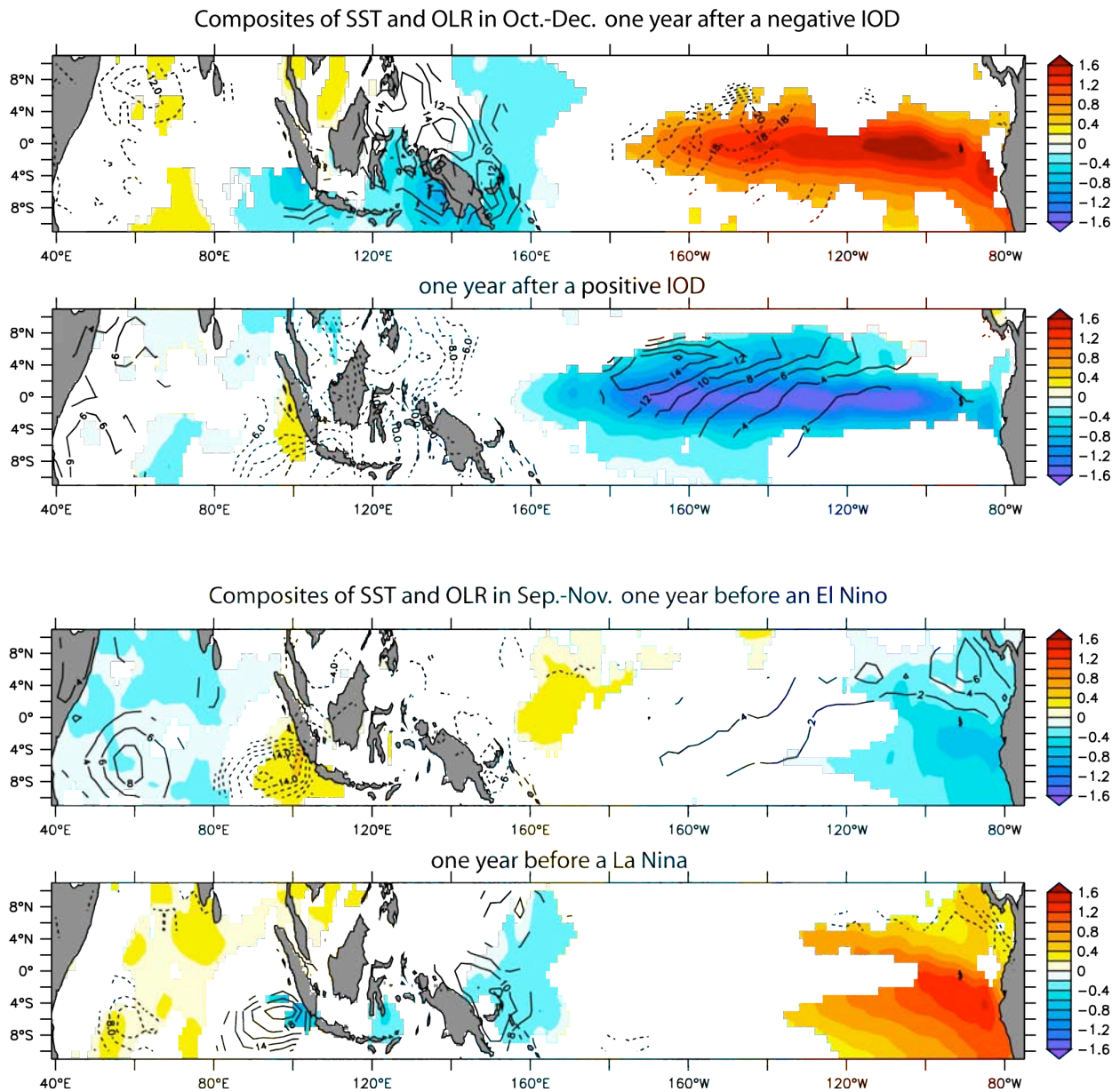
Fig. S6. Upper panels: composites of SST (colours, ºC) and OLR (contours, W m^{-2}) in Oct-Dec one year after a negative (positive) IOD. **Lower panels:** composites for Sept-Nov one year before an El Niño (La Niña) event. Only signals significant at the 90% level are shown. The upper panels confirm that a negative (positive) IOD event tends to favour El Niño (La Niña) conditions the following year. The lower panels confirm that El Niño (La Niña) conditions tend to be preceded by a negative (positive) IOD event the year before.

Supplementary Tables

Lead-correl. with Niño3.4 SST in Oct.-Dec. one year later for various periods and IOD indices:	Lead-correl. (signif.)
Over 1956-2008 using: DMI	-0.47 (99%)
IOI	-0.45 (99%)
Over 1974-2008 using OLR-IOD index	-0.58 (99%)
Over 1981-2008 using:	
DMI from OISSTV2	-0.54 (99%)
DMI from HadiSST	-0.55 (99%)
DMI from ERSSTV3b	-0.49 (99%)
DMI from HadSST2	-0.48 (99%)
OLR-IOD index	-0.63 (99%)
IOI	-0.50 (99%)
Over 1956-1980 using:	
DMI from HadiSST	-0.36 (90%)
DMI from ERSSTV3b	-0.31 (80%)
DMI from HadSST2	-0.41 (95%)
IOI	-0.40 (95%)

Table S1: Lead-correlations (and significance level) between the IOD index in fall (Sept-Nov) and the following year ENSO (Niño3.4 SST in Oct-Dec, so a 13 month lead), for different periods, SST products and IOD indices (see section 2.4a). Note that HadSST2 is an uninterpolated product using only in situ SST data.

Predicting different ENSO indices in Oct.-Dec. one year later, using OLR-based IOD + WWV in Oct. (DMI+WWV in Sep.-Nov.), over Sep.1981-Dec.2008 (27 years), for:	Hindcast corr. skill	Simple lag-correlation with OLR-based IOD (DMI)
Niño4 SST	0.88 (0.82)	-0.52 (-0.64)
Niño3.4 SST	0.87 (0.82)	-0.65 (-0.54)
Niño3 SST	0.81 (0.75)	-0.48 (-0.59)
Niño1+2 SST	0.63 (0.56)	-0.46 (-0.35)
For Southern Oscillation Index:		
SOI	0.77 (0.66)	0.57 (0.40)
SOI*	0.81 (0.71)	0.63 (0.48)
For Western Pacific indices:		
Niño5 SST (equatorial Western Pacific)	0.68 (0.57)	0.62 (0.49)
Niño6 SST (Northwest Pacific)	0.67 (0.54)	0.63 (0.49)
For "Modoki (warm pool)" El Niño:		
El Niño Modoki Index (EMI)	0.72 (0.67)	-0.56 (-0.46)

Table S2. Skill of the bilinear regression model for different ENSO indices First column: correlation skill of the bilinear hindcasts of the ENSO peak (Oct-Dec SST) using 13 month lead "best predictor" (see section 2.1.a), i.e. OLR-based IOD + WWV in Oct. (and in parentheses using DMI and WWV in Sep.-Nov.). Second column: the simple lag-correlation between the IOD index and next year's ENSO peak. The first lines are for various Niño regions in the central to eastern Pacific, and then for the Southern Oscillation Index (SOI, and also SOI* with periods lower than 6 months filtered to remove atmospheric noise). Then correlation skills for western Pacific indices are given. And finally for the warm pool El Niño Modoki index [e.g. Ashok et al. 2007]. The best skills of the bilinear regression are found for Niño4, Niño3.4 and Niño3 SST regions. But the regression remains significantly efficient also for the other indices (with an opposite sign of the IOD influence for western Pacific SST indices), and particularly for the El Niño Modoki index (that could help to determine the type/"flavour" of El Niño).